Nanoscale

PAPER

View Article Online
View Journal

Cite this: DOI: 10.1039/c4nr05384b

Phosphorene oxide: stability and electronic properties of a novel two-dimensional material†

Gaoxue Wang,[a] Ravindra Pandey*[a] and Shashi P. Karna[b]

Received 15th September 2014,
Accepted 28th October 2014

DOI: 10.1039/c4nr05384b

www.rsc.org/nanoscale

Phosphorene, the monolayer form of (black) phosphorus, was recently exfoliated from its bulk counterpart. Phosphorene oxide, by analogy to graphene oxide, is expected to have novel chemical and electronic properties, and may provide an alternative route to the synthesis of phosphorene. In this research, the physical and chemical properties of phosphorene oxide including its formation by oxygen adsorption on the bare phosphorene was investigated. Analysis of the phonon dispersion curves finds stoichiometric and non-stoichiometric oxide configurations to be stable at ambient conditions, thus suggesting that the oxygen adsorption may not degrade the phosphorene. The nature of the band gap of the oxides depends on the degree of functionalization of phosphorene; an indirect gap is predicted for the non-stoichiometric configurations, whereas a direct gap is predicted for the stoichiometric oxide. Application of mechanical strain or an external electric field leads to tunability of the band gap of the phosphorene oxide. In contrast to the case of the bare phosphorene, dependence of the diode-like asymmetric current–voltage response on the degree of stoichiometry is predicted for the phosphorene oxide.

1. Introduction

Two-dimensional (2D) materials have been extensively studied because of their novel properties and important technological applications. In particular, the discovery of graphene has stimulated an avalanche of investigations to exploit its novel properties for applications at the nanoscale.[1] In the post-silicon era, graphene has been widely regarded as the most promising building block for electronic devices. However, its metallic nature together with its sensitivity to the environment leads to a somewhat limited scope of application. A finite band gap in a material is known to be essential for the fabrication of device elements including transistors. The limitations associated with graphene have led to exploration of 2D materials beyond graphene.[2]

Phosphorene has recently attracted attention as an alternative to graphene because of its direct band gap of 2 V and its large current on/off ratio with a hole mobility of about 1000 $cm^2\ V^{-1}\ s^{-1}$ (ref. 3–5). Fabrication of phosphorene-based optical devices with broadband photo responses has recently been reported.[6,7] Note that phosphorene is successfully exfoliated from the most stable allotrope of phosphorus, black phosphorus.[3,8,9]

The chemical modification of 2D materials has now routinely been performed to tailor their physical, chemical and electronic properties. In the case of graphene, surface modifications by H, O, and F atoms often lead to substantial changes in its electronic structure. For example, H- and F-functionalized graphene are wide band gap materials, whereas graphene has a zero gap at the Dirac point.[10–12] Also, graphene oxides are the structures in which oxygen functional groups are present and as a result have remarkable mechanical strength and tunable optoelectronic properties and also have a broad usage for the large scale fabrication of graphene.[13–16] Furthermore, a recent paper argues that the oxidation of phosphorene will result in its degradation by the formation of molecular compounds such as phosphorus trioxide (P_4O_6), and phosphorus pentoxide (P_4O_{10}) or phosphates.[17,18] However, such conjecture has not yet been verified by experimental or theoretical studies.

In this letter, the results of a theoretical study based on density functional theory on the oxide configurations of phosphorene are presented. The interaction of oxygen in both atomic and molecular form with the bare phosphorene is investigated first, and this predicts the preferred binding site and energy barrier to dissociate the oxygen molecule adsorbed on the monolayer. The effect of the degree of oxygen functionalization on the stability and electronic structure of phosphorene are also examined. The transverse electron transport properties of the oxide configurations are calculated in a

[a]Department of Physics, Michigan Technological University, Houghton, Michigan 49931, USA. E-mail: gaoxuew@mtu.edu, pandey@mtu.edu, shashi.p.karna.civ@mail.mil
[b]US Army Research Laboratory, Weapons and Materials Research Directorate, ATTN: RDRL-WM, Aberdeen Proving Ground, MD 21005-5069, USA
† Electronic supplementary information (ESI) available. See DOI: 10.1039/c4nr05384b

model setup mimicking the scanning tunneling microscopy (STM) experiment.

2. Computational details

Electronic structure calculations were performed using the density functional theory (DFT) method using the norm-conserving Troullier–Martins pseudopotential as implemented in SIESTA.[19] The Perdew–Burke–Ernzerhof (PBE)[20] exchange correlation functional was employed. A double zeta basis including polarization orbitals was used. The energy convergence was set to 10^{-5} eV. The mesh cutoff energy was chosen to be 500 Ry. The geometry optimization was considered to be converged when the residual force on each atom was smaller than 0.01 eV $Å^{-1}$. In our periodic supercell approach, the vacuum distance normal to the plane was larger than 20 Å to eliminate interaction between the replicas. A dipole correction was employed to eliminate the artificial electrostatic field between the periodic supercells.

For calculations describing the interaction of an O atom and an O_2 molecule with phosphorene, a (3 × 4) supercell with a total of 48 P atoms was used and the reciprocal space was sampled by a grid of (5 × 5 × 1) *k* points in the Brillouin zone. Additionally, PO, P_2O_1 and P_4O_1 configurations were calculated with a (1 × 1) supercell consisting of 4 P atoms, and the P_8O_1 configuration was calculated with a (1 × 2) supercell consisting of 8 P atoms. The *k*-point mesh of (11 × 11 × 1) was used for these oxide configurations. The phonon dispersion calculation was based on the Vibra package of the SIESTA utility.[21]

Phosphorene has a puckered surface because of the sp^3 character of the chemical bonds at the surface. The bond lengths and the bond angles were found to be 2.29 Å, 2.26 Å and 103.7°, 95.6°, respectively which are in agreement with the previously reported values obtained at the PBE-DFT level of theory.[22,23] Likewise, calculations using the same modeling elements reproduced the structural and electronic properties of graphene-based systems,[24–27] thereby showing the accuracy and reliability of this computational model in describing 2D materials.

3. Results and discussion

3.1 Monoatomic oxygen (O)

Firstly, the interaction of a single oxygen atom with phosphorene was investigated. Fig. 1 shows the lattice sites considered for the oxygen approaching the phosphorene: (i) the ring site – above the center of the hexagonal ring, (ii) the top site – above the top of the P atom, and (iii) the bridge site – above the bridge of the P–P bonds. Interestingly, the O atoms approaching either the top or ring sites prefer the same equivalent positions in their equilibrium configurations, which have a tetrahedral coordination for P atoms.

In the equilibrium configuration, $R_{(P–O)}$ is ~1.54 Å, and the binding energy/oxygen atom defined as $(E_{(Phosphorene)} + E_{(O_2\ molecule)}/2 - E_{(Phosphorene+O\ atom)})$ is calculated to be 1.4 eV per oxygen atom. The bridge site configuration is ~2.3 eV higher in energy than the equilibrium configuration which is in contrast to graphene oxide where the bridge site is found to be the preferred binding site for oxygen.[16] The adsorbed oxygen atom does not induce either magnetism or mid-gap states as shown by the spin polarized density of states (DOS), see ESI, Fig. S1.†

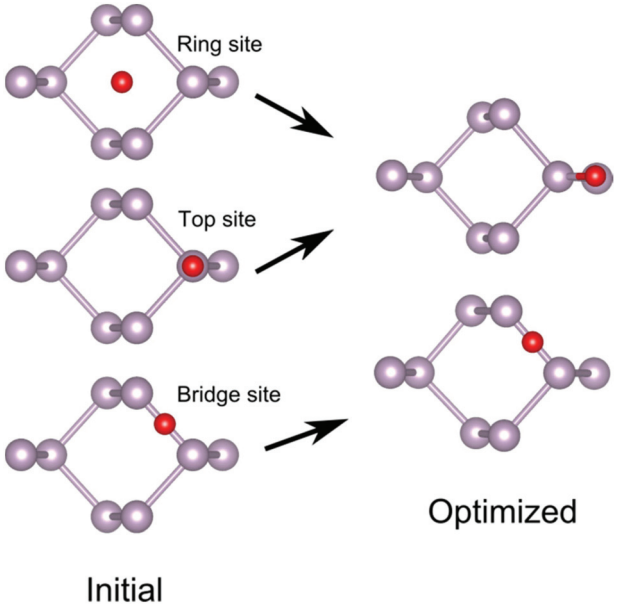

Fig. 1 Single oxygen atom adsorption on phosphorene. The left panel shows the initial configurations and the right panel shows the optimized configurations. The oxygen atoms are in red, and the phosphorus atoms are in purple.

3.2 Molecular oxygen (O_2)

Next, the interaction of an oxygen molecule with phosphorene was investigated, considering both adsorption and dissociation processes on the surface. Fig. 2(a) shows the calculated ground state configuration of the adsorbed oxygen molecule. Here, O_2 prefers a tilted orientation with $R_{(P–O1)}$ = 1.69 Å and $R_{(P–O2)}$ = 1.75 Å. Note that the adsorbed O_2 gets stretched out on the surface with $R_{(O–O)}$ of 1.60, which is substantially larger than that of O_2 (~1.24 Å). The binding energy defined as $(E_{(Phosphorene)} + E_{(O_2\ molecule)} - E_{(Phosphorene+O_2\ molecule)})$ is found to be about 0.78 eV per oxygen molecule. The binding energy of an oxygen molecule is smaller than the binding energy of two separated oxygen atoms because of the energy needed to stretch $R_{(O–O)}$ to 1.60 Å. Note that the spin polarization was considered for the binding energy calculations.

The dissociation process of the adsorbed O_2 is simulated by fixing an O atom (*i.e.*, O1), and moving the other atom (*i.e.* O2) laterally in the unit cell (shadowed region) as shown in the inset of Fig. 2(a). A minimum occurs in the corresponding energy surface as shown in Fig. 2(b) when O2 moves toward the P2 site. The calculated energy barrier is 0.33 eV along the path illustrated by the arrows in Fig. 2(c). The energy barrier increases to 1.31 eV when O2 is moved to a new atomic site,

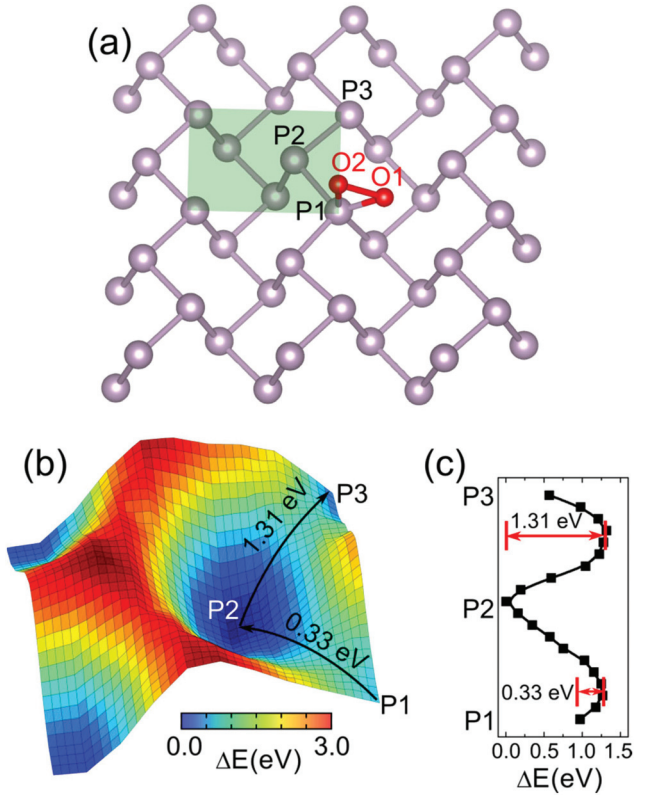

Fig. 2 O_2 on phosphorene: (a) the ground state configuration, (b) the energy surface showing displacement of an O atom from P1 to P2 to P3 atomic sites, and (c) the calculated energy barrier along the paths as shown by the arrows in (b). The oxygen atoms are in red, and the phosphorus atoms are in purple.

P3. In an alternative scenario of moving the O1 atom and fixing the O2 atom, a much higher energy barrier is expected because the O1 atom is strongly bonded to a P atom with the bond distance of 1.03 Å (see ESI, Fig. S2†). Note that the dissociation energy of an O_2 molecule on bare graphene is about 2.39 eV,[28] which is much larger than the dissociation energy of the O_2 molecule on phosphorene (~0.3 eV). Dissociation of the adsorbed O_2 on phosphorene can, therefore, be one of the possible chemical routes to form the phosphorene oxide.[18]

3.3. Stoichiometric phosphorene oxide (PO)

Phosphorene has a puckered surface (Fig. 3(a)), and addition of an O atom at each atomic site leads to a configuration of PO with a slight increase in the P–P bond lengths (2.32, 2.37 Å) as compared to those for the bare phosphorene. The length of the P–O bond is 1.51 Å (Fig. 3(b)) which is similar to the C–O bond length of 1.47 Å in graphene oxide,[29] and is slightly larger than the B–O distance of 1.40 Å for O_2 adsorbed on a B_{13} cluster.[30]

As seen from the side view of Fig. 3(b), PO is deformed compared to the bare phosphorene with changes in bond angles between the P atoms. However, the structure retains its original configuration without cleavage of P–P bonds. This is different from the cases of H, F, and –OH adsorption which act as chemical scissors and break phosphorene down into nanoribbons.[31]

In the stoichiometric PO configuration, the ∠P–P–P bond angles are 121.2°, 93.6° and 100.9°. The change in the ∠P–P–P bond angles, relative to the bare phosphorene, is closely related to the charge redistribution as shown in the deformation

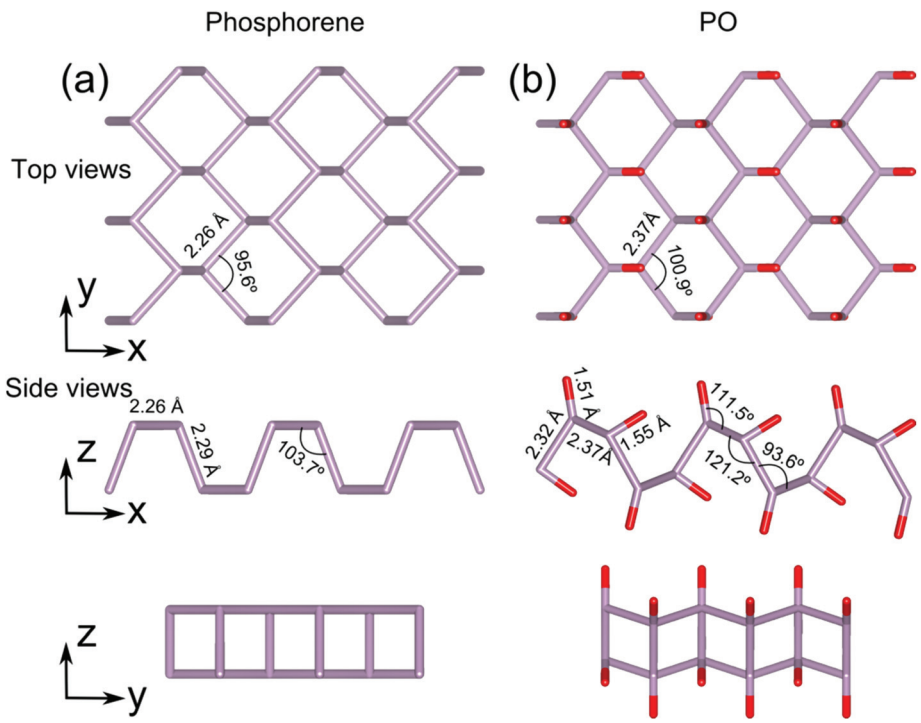

Fig. 3 Top and side views of (a) phosphorene, and (b) phosphorene oxide.

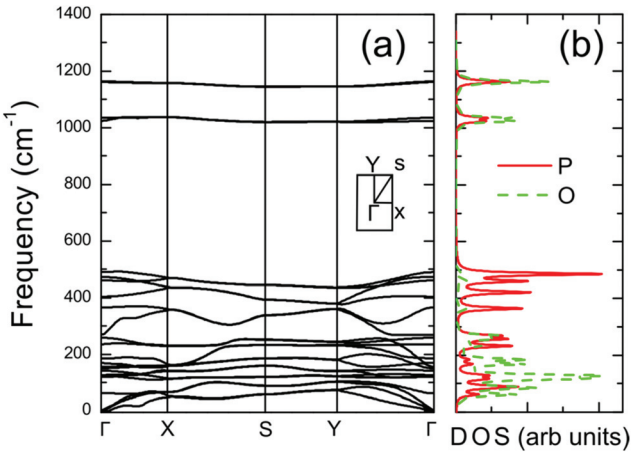

Fig. 4 Phosphorene oxide: (a) the phonon dispersion curves, and (b) density of states.

charge density plot, see ESI, Fig. S3.† Analysis of the Mulliken charges finds that ~0.2 *e* is transferred from a P atom to an O atom. This is different from graphene oxide where O tends to bind on the bridge of a C–C bond forming epoxy group, and the accumulated electron density around O comes from the two neighboring C atoms of graphene[29,32,33]

The stability of the phosphorene oxide is confirmed by the calculated phonon dispersion curves showing no negative frequencies (Fig. 4). The phonon dispersion of PO is greatly different from that of phosphorene and it can be grouped into three regions (Fig. 4(b)) with the highest vibrational frequency at about ~1160 cm^{-1}. Furthermore, the phonon dispersion curves of the bare phosphorene have separated acoustic and optical modes with the maximum vibrational frequency at ~460 cm^{-1}. In the lower acoustic region for PO, the vibrational modes are associated with the constituent P and O atoms. The modes associated with the P atoms dominate in the middle region of the spectrum. The high frequency modes correspond to the P–O stretching modes indicating a relatively high strength for the P–O bond in the 2D lattice.

In our study, the oxygen adsorption on phosphorene is considered to be more like an ordered adsorption of adsorbates on graphene, such as in the case of graphane, fluorographene, and chlorographene.[10,12,34] In graphene oxide, the oxygen functional groups form an inhomogeneous lattice which is revealed by TEM measurements.[33] This may be because of the interaction of oxygen atoms at the top and bottom sides of graphene leading to a clustering of oxygen atoms. A recent theoretical study predicts the formation of ordered, homogeneous single surface graphene oxides by oxidizing only the top layer of graphene.[16] Formation of homogeneous graphene oxides is also observed after the oxidation of epitaxial graphene grown on a silicon carbide substrate.[35]

The calculated band structure of PO is shown in Fig. 5. The valence band maximum (VBM) has a p_y character associated with both P and O atoms (Fig. 5(c)), and the conduction band minimum (CBM) is formed by P-s orbitals and O-p_z orbitals (Fig. 5(c)). The calculated band gap is direct at Γ with a value

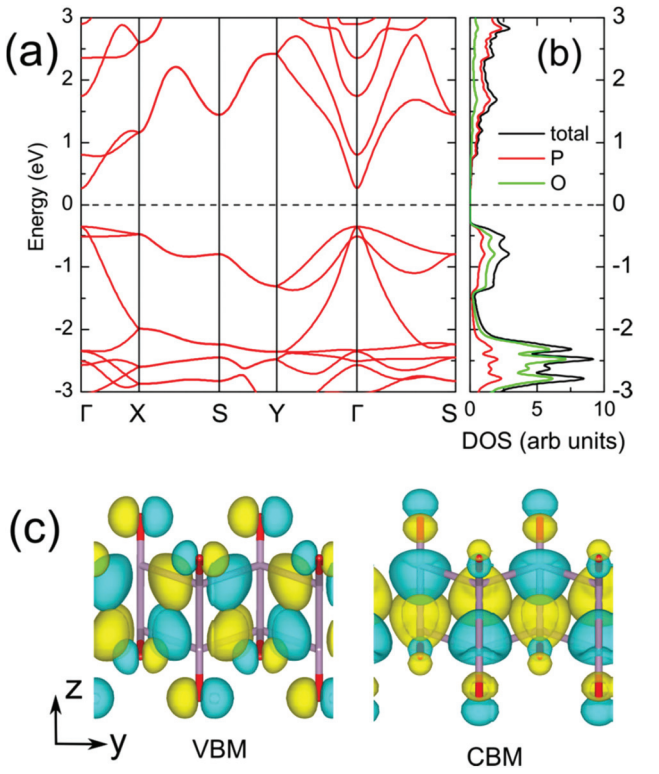

Fig. 5 Electronic properties of phosphorene oxide: (a) band structure, (b) density of states, and (c) Kohn–Sham wave functions at Γ associated with states corresponding to the top of the VBM and the bottom of the CBM. Γ, S, Y and X in the *k*-space are defined as (0,0,0), (1/2,1/2,0), (0,1/2,0), and (1/2,0,0), respectively.

of ~0.6 eV. It is smaller in magnitude than that calculated for the bare phosphorene (~1 eV at the PBE-DFT level of theory). Anisotropy in the band structure of the 2D lattice is predicted; the hole effective masses are 4.56 and 1.74 m_e along the Γ–X and Γ–Y directions, respectively. In contrast, the electron effective mass does not show anisotropy and has a magnitude of 0.18 m_e (see ESI, Fig. S4†).

Application of tensile strain along the *x* direction of phosphorene oxide yields a linear variation of the band gap across a range of values (0.1–0.6 eV) for the strain values of 0% to 8% (Fig. 6(a)). The predicted variation in the band gap is mainly due to variation of the CBM at Γ (see ESI, Fig. S5 and S6†). The top of the VBM, which is mainly formed by the oxygen atoms does not appear to be sensitive to the external strain (see ESI, Fig. S6†). The application of an external electric field modifies the band gap of phosphorene oxide, reducing it to 0.4 eV at 1.5 V Å^{-1}, whereas it does not change the band gap for the bare phosphorene (Fig. 6(b)). This is because of the reduced symmetry in the oxide configuration compared to its bare configuration. Thus, the oxygen functionalization of phosphorene yields tunability of the band gap with both tensile strain and electric field.

The in-plane stiffness of the 2D lattice is calculated by fitting the strain energy within the strain range of −2% to 2% (see ESI, Fig. S7†).[24] The calculated stiffness constants for

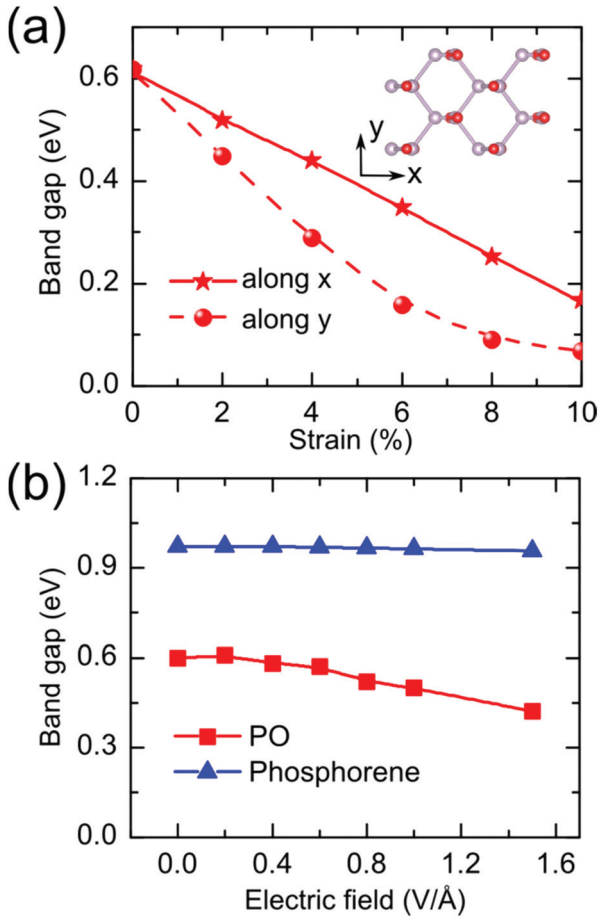

Fig. 6 Phosphorene oxide: (a) band gap *versus* in-plane tensile strain, and (b) band gap *versus* electric field applied perpendicular to the 2D lattice.

phosphorene are 21 N m^{-1} and 66 N m^{-1} along the x and y directions, respectively. For the phosphorene oxide, the stiffness constants are decreased to 16 N m^{-1} and 33 N m^{-1} along the x and y directions because of the increased P–P bond length in the oxide lattice. These values are much smaller than those associated with graphene (340 N m^{-1} (ref. 36)) and suggest the softness of phosphorene-based 2D materials.[37]

3.4 Non-stoichiometric phosphorene oxide

Next the stabilities and electronic properties of non-stoichiometric phosphorene oxides representing the cases of partial functionalization of phosphorene were investigated. Fig. 7 shows the considered non-stoichiometric oxide configurations including P_8O_1 (*i.e.*, $PO_{0.125}$), P_4O_1 (*i.e.*, $PO_{0.25}$), and P_2O_1 (*i.e.*, $PO_{0.5}$), with a single side adsorption of the oxygen atoms.

Fig. 8 shows the variation of the band gap with the degree of functionalization of phosphorene. Bare phosphorene is a direct gap 2D material. This is not the case with phosphorene oxides where the nature of the band gap depends on the degree of functionalization and an indirect band gap is predicted for $PO_{0.125}$, $PO_{0.25}$, and $PO_{0.5}$. Finally, a crossover from an indirect to a direct band gap is seen for the stoichiometric PO configuration. The direct band gap is defined as the energy gap at Γ. Because the location of VBM and CBM depends on the degree of functionalization of phosphorene (see ESI, Fig. S8†), the indirect band gap is defined as (Γ→Γ–Y), (Γ→Γ–X), (S→Y), (Γ→Γ–X), and (Γ→Γ–X) for P, $PO_{0.125}$, $PO_{0.25}$, $PO_{0.5}$ and PO, respectively.

The phonon dispersion curves of non-stoichiometric configurations (see ESI, Fig. S8†) suggest the stability of the partially oxidized configurations, though small negative values

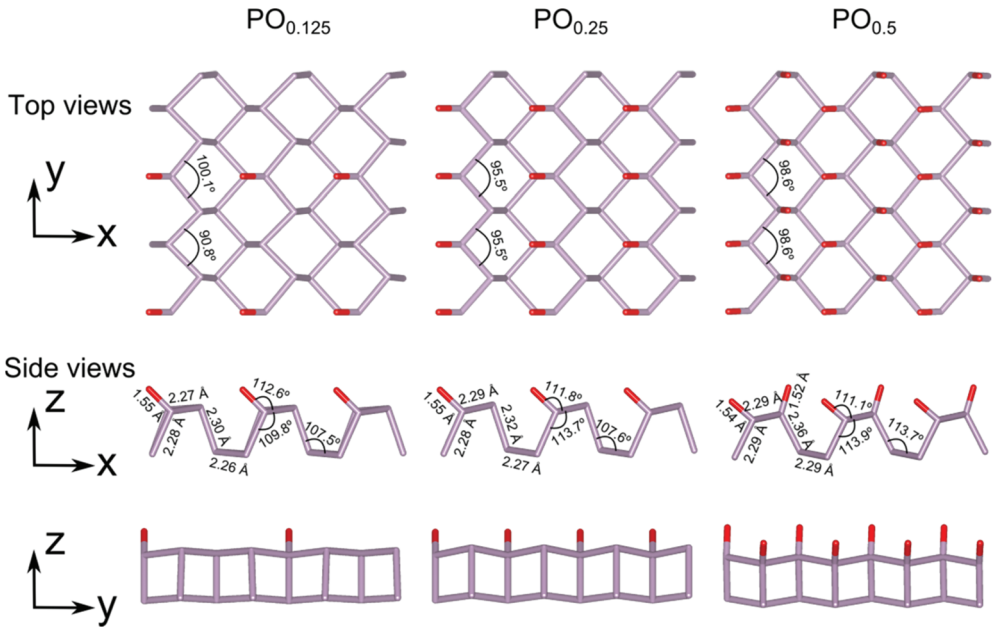

Fig. 7 Structures of non-stoichiometric oxide configurations: $PO_{0.125}$, $PO_{0.25}$, and $PO_{0.5}$.

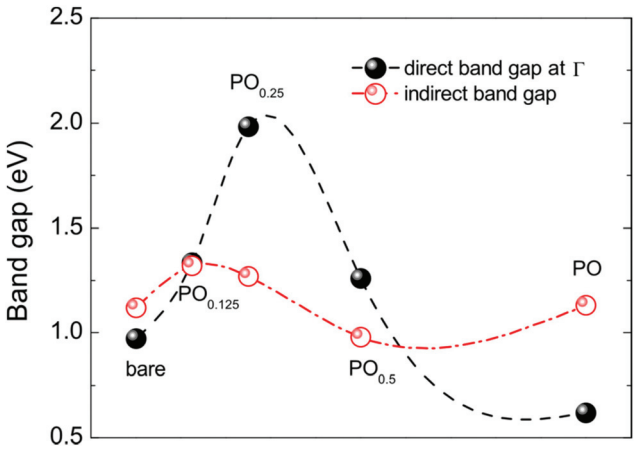

Fig. 8 The variation of band gap as a degree of functionalization of the bare phosphorene. Open and solid circles represent the values of indirect and direct band gaps, respectively. The direct band gap is taken to be at Γ.

($\sim$8 cm^{-1}) near Γ may be an artifact of the numerical approximation employed in the frequency calculations.

The work function is a crucial physical quantity for determining the emission properties of materials and has a considerable impact on device performance. It is defined as the energy difference between the vacuum level and the Fermi energy. For the oxide configurations, the work function shows a steady increase with the increased degree of oxygen functionalization of the bare phosphorene. This is because of the fact that the charge transfer from P to O as shown by the deformation charge density plot (see ESI, Fig. S3†) leads to the formation of dipoles between the phosphorus layer and oxygen layer, thus preventing electrons from moving towards the vacuum. The calculated values of the work function for bare phosphorene, $PO_{0.125}$, $PO_{0.25}$, $PO_{0.5}$, and PO are 4.5, 4.9, 5.2, 5.8, and 7.2 eV, respectively. Therefore, the work function can be tailored effectively by the degree of oxygen functionalization of phosphorene. A similar tunable work function has already been reported for graphene where the work function increases

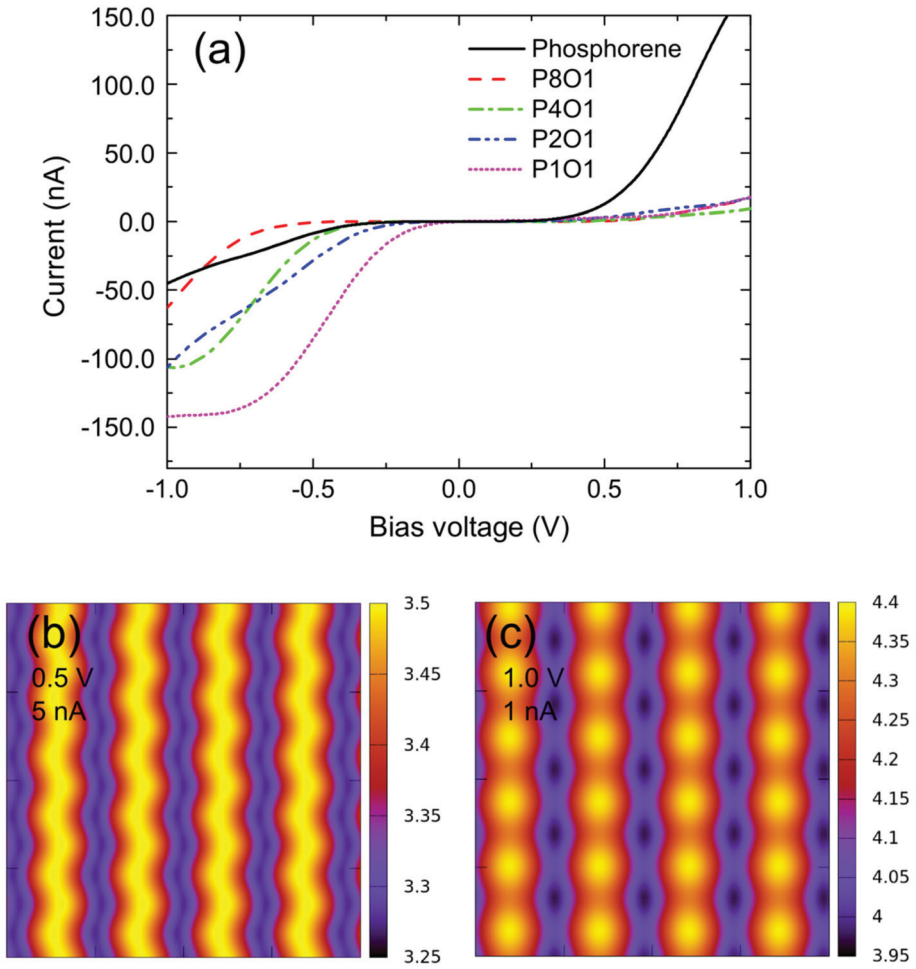

Fig. 9 (a) Tunneling characteristics of the phosphorene oxide configurations. (b) The simulated STM image of phosphorene and (c) the simulated STM image of phosphorene oxide. The current is calculated using a Au13 tip located at 3 Å above the surface. The side scale bar shows the distance from the tip to the surface in Å.

from 4.2 eV to 5.5 eV with 20% concentration of oxygen functionalization.[38,39]

3.5 Tunneling characteristics

Finally, the tunneling characteristics of the phosphorene oxides were investigated. The tunneling current from the sample to the tip at $\vec{r}_t$ location based on the Tersoff and Hamann approximation[40] is:

$$I(\vec{r}_t; V) \approx \frac{2\pi e}{\hbar}\int_{-\infty}^{+\infty} \rho_t\left(E - \frac{eV}{2}\right)\rho_s\left(\vec{r}_t; E + \frac{eV}{2}\right)F(E)\mathrm{d}E \quad (1)$$

where ρ_t is the electron density of the tip and ρ_s is the electron density of the sample at the location of the tip. $F(E)$ is the term which includes the effect of thermally excited electrons as proposed by He *et al.*[41–44] In order to mimic the STM measurements, the constant current mode is used with the gold tip represented by a Au_{13} cluster. The size of the STM images are (20 Å × 20 Å), and a positive bias between the sample and the tip is applied. It is to be noted here that a positive bias between the sample and the tip will lead to tunneling of electrons from tip-VB to sample-CB. With a negative bias, the electrons will tunnel from sample-VB to tip-CB (see ESI, Fig. S9†).

The electron transport studies offer some intriguing insights into electron tunneling in the direction perpendicular to the stable phosphorene oxide plane. Asymmetric current–voltage semiconducting characteristics (Fig. 9(a)) are seen for both stoichiometric and non-stoichiometric oxide configurations. Bare phosphorene shows a strong diode-like behavior with a large tunneling current in the positive bias regime. Upon oxygen adsorption, this behavior completely changes, with high current in the negative bias regime. The high tunneling current of PO in the negative bias region is because of the contribution of oxygen atoms in the top of the valance band (Fig. 5(b)).

The dependence of the threshold voltage onset of the tunneling current on the degree of functionalization suggests that tunable electronic properties can be achieved by the oxygen functionalization of phosphorene. In the negative bias region, the threshold voltage decreases from −0.55 V (P_8O_1) to −0.15 V (PO) (Fig. 9(a)) which is related to the variation in the band gap of oxides. Furthermore, the STM images as seen in Fig. 9(b) and (c) can help in identifying the formation of the phosphorene oxide from the bare phosphorene.

Summary

The interaction of phosphorene with oxygen and the formation of 2D phosphorene oxide were investigated with the use of the DFT. A number of key findings have emerged from this study based on DFT. Firstly, our calculations predict that the 2D phosphorene oxide is stable in both stoichiometric and non-stoichiometric configurations. Secondly, a fully functionalized phosphorene is a direct band gap material with band gaps that are tunable by external strain and electric field. Partially functionalized phosphorene has an indirect band gap. Thirdly, the dissociation energy of an oxygen molecule is calculated to be ~0.33 eV, suggesting the possible, low energy oxidation of phosphorene which is likely to lead to the 2D phosphorene-based structures. Finally, electron transport studies offer some intriguing insights into electron tunneling in the direction perpendicular to the phosphorene oxide plane with dependence of the current on the degree of functionalization of phosphorene. It is believed that the results of this study will inspire experimental efforts into the study and synthesis of electronic devices using phosphorene oxide.

Acknowledgements

The authors thank D.R. Banyai for providing his STM simulation code, and are grateful to Dr S. Gowtham for his support with the installation of the required software. RAMA and Superior high performance computing clusters at the Michigan Technological University were used in obtaining the results presented in this paper. Financial support from ARL W911NF-14-2-0088 is acknowledged.

References

1 K. S. Novoselov, *et al.*, Electric field effect in atomically thin carbon films, *Science*, 2004, **306**(5696), 666–669.
2 S. Z. Butler, *et al.*, Progress, Challenges, and Opportunities in Two-Dimensional Materials Beyond Graphene, *ACS Nano*, 2013, **7**(4), 2898–2926.
3 L. Li, *et al.*, Black phosphorus field-effect transistors, *Nat. Nanotechnol.*, 2014, **9**(5), 372–377.
4 H. Liu, *et al.*, Phosphorene: An Unexplored 2D Semiconductor with a High Hole Mobility, *ACS Nano*, 2014, **8**(4), 4033–4041.
5 J. Qiao, *et al.*, *Few-layer black phosphorus: emerging direct band gap semiconductor with high carrier mobility*, arXiv preprint arXiv:1401.5045, 2014.
6 M. Buscema, *et al.*, Fast and Broadband Photoresponse of Few-Layer Black Phosphorus Field-Effect Transistors, *Nano Lett.*, 2014, **14**(6), 3347–3352.
7 T. Low, *et al.*, *Tunable optical properties of multilayers black phosphorus*, arXiv preprint arXiv:1404.4030, 2014.
8 C.-G. Andres, *et al.*, Isolation and characterization of few-layer black phosphorus, *2D Mater.*, 2014, **1**(2), 025001.
9 F. Xia, H. Wang and Y. Jia, *Rediscovering Black Phosphorus: A Unique Anisotropic 2D Material for Optoelectronics and Electronics*, arXiv preprint arXiv:1402.0270, 2014.
10 D. C. Elias, *et al.*, Control of Graphene's Properties by Reversible Hydrogenation: Evidence for Graphane, *Science*, 2009, **323**(5914), 610–613.
11 R. R. Nair, *et al.*, Fluorographene: A Two-Dimensional Counterpart of Teflon, *Small*, 2010, **6**(24), 2877–2884.
12 K.-J. Jeon, *et al.*, Fluorographene: A Wide Bandgap Semiconductor with Ultraviolet Luminescence, *ACS Nano*, 2011, **5**(2), 1042–1046.

13 G. Eda and M. Chhowalla, Chemically Derived Graphene Oxide: Towards Large-Area Thin-Film Electronics and Optoelectronics, *Adv. Mater.*, 2010, **22**(22), 2392–2415.
14 J. T. Robinson, *et al.*, Wafer-scale reduced graphene oxide films for nanomechanical devices, *Nano Lett.*, 2008, **8**(10), 3441–3445.
15 J. T. Robinson, *et al.*, Reduced graphene oxide molecular sensors, *Nano Lett.*, 2008, **8**(10), 3137–3140.
16 B. Huang, *et al.*, Overcoming the Phase Inhomogeneity in Chemically Functionalized Graphene: The Case of Graphene Oxides, *Phys. Rev. Lett.*, 2013, **110**(8), 085501.
17 S. P. Koenig, *et al.*, Electric field effect in ultrathin black phosphorus, *Appl. Phys. Lett.*, 2014, **104**(10), 103106.
18 A. Ziletti, *et al.*, *Oxygen defects in phosphorene*, arXiv preprint arXiv:1407.5880, 2014.
19 M. S. José, *et al.*, The SIESTA method for ab initio order-N materials simulation, *J. Phys.: Condens. Matter*, 2002, **14**(11), 2745.
20 J. P. Perdew, K. Burke and M. Ernzerhof, Generalized Gradient Approximation Made Simple, *Phys. Rev. Lett.*, 1996, **77**(18), 3865–3868.
21 A. Postnikov, O. Pagès and J. Hugel, Lattice dynamics of the mixed semiconductors (Be, Zn) Se from first-principles calculations, *Phys. Rev. B: Condens. Matter*, 2005, **71**(11), 115206.
22 A. S. Rodin, A. Carvalho and A. H. Castro Neto, Strain-Induced Gap Modification in Black Phosphorus, *Phys. Rev. Lett.*, 2014, **112**(17), 176801.
23 J. Guan, Z. Zhu and D. Tománek, *Phase coexistence and metal-insulator transition in few-layer phosphorene: A computational study*, arXiv preprint arXiv:1407.1894, 2014.
24 G. Wang, *et al.*, Strain engineering of Dirac cones in graphyne, *Appl. Phys. Lett.*, 2014, **104**(21), 213107.
25 X. Zhong, *et al.*, First-principles study of strain-induced modulation of energy gaps of graphene/BN and BN bilayers, *Phys. Rev. B: Condens. Matter*, 2011, **83**(19), 193403.
26 X. Zhong, *et al.*, Electronic structure and quantum transport properties of trilayers formed from graphene and boron nitride, *Nanoscale*, 2012, **4**(17), 5490–5498.
27 X. Zhong, R. Pandey and S. P. Karna, Stacking dependent electronic structure and transport in bilayer graphene nanoribbons, *Carbon*, 2012, **50**(3), 784–790.
28 H. Yan, *et al.*, First-principles study of the oxygen adsorption and dissociation on graphene and nitrogen doped graphene for Li-air batteries, *J. Appl. Phys.*, 2012, **112**(10), 104316.
29 Y. Dai, *et al.*, Diffusion and desorption of oxygen atoms on graphene, *J. Phys.: Condens. Matter*, 2013, **25**(40), 405301.
30 W. J. Slough, A. K. Kandalam and R. Pandey, Reactivity of neutral and charged B13 clusters with O2: A theoretical study, *J. Chem. Phys.*, 2010, **132**(10), 104304.
31 X. Peng and Q. Wei, *Chemical scissors cut phosphorene nanostructures and their novel electronic properties*, arXiv preprint arXiv:1405.0801, 2014.
32 J. Ito, J. Nakamura and A. Natori, Semiconducting nature of the oxygen-adsorbed graphene sheet, *J. Appl. Phys.*, 2008, **103**(11), 113712.
33 M.-T. Nguyen, R. Erni and D. Passerone, Two-dimensional nucleation and growth mechanism explaining graphene oxide structures, *Phys. Rev. B: Condens. Matter*, 2012, **86**(11), 115406.
34 H. Sahin and S. Ciraci, Chlorine Adsorption on Graphene: Chlorographene, *J. Phys. Chem. C*, 2012, **116**(45), 24075–24083.
35 M. Z. Hossain, *et al.*, Chemically homogeneous and thermally reversible oxidation of epitaxial graphene, *Nat. Chem.*, 2012, **4**(4), 305–309.
36 C. Lee, *et al.*, Measurement of the Elastic Properties and Intrinsic Strength of Monolayer Graphene, *Science*, 2008, **321**(5887), 385–388.
37 Q. Wei and X. Peng, *Superior mechanical flexibility of phosphorene and few-layer black phosphorus*, arXiv preprint arXiv:1403.7882, 2014.
38 P. V. Kumar, M. Bernardi and J. C. Grossman, The Impact of Functionalization on the Stability, Work Function, and Photoluminescence of Reduced Graphene Oxide, *ACS Nano*, 2013, **7**(2), 1638–1645.
39 A. Misra, H. Kalita and A. Kottantharayil, Work Function Modulation and Thermal Stability of Reduced Graphene Oxide Gate Electrodes in MOS Devices, *ACS Appl. Mater. Interfaces*, 2013, **6**(2), 786–794.
40 J. Tersoff and D. R. Hamann, Theory and Application for the Scanning Tunneling Microscope, *Phys. Rev. Lett.*, 1983, **50**(25), 1998–2001.
41 H. He, *et al.*, Spin-polarized electron transport of a self-assembled organic monolayer on a Ni(111) substrate: An organic spin switch, *Phys. Rev. B: Condens. Matter*, 2006, **73**(19), 195311.
42 S. K. Gupta, *et al.*, Electron tunneling characteristics of a cubic quantum dot, (PbS) 32, *J. Chem. Phys.*, 2013, **139**(24), 244307.
43 A. Kumar, *et al.*, Electronic stability and electron transport properties of atomic wires anchored on the MoS 2 monolayer, *Phys. Chem. Chem. Phys.*, 2014, **16**(37), 20157–20163.
44 S. K. Gupta, *et al.*, Effect of Si doping on the electronic properties of BN monolayer, *Nanoscale*, 2014, **6**(10), 5526–5531.

